JOURNAL OF SOLID STATE CHEMISTRY 16, 97–116 (1976)

Chalkogenides of the Transition Elements. X. X-Ray, Neutron, Mössbauer, and Magnetic Studies of Pentlandite and the π Phases π(Fe, Co, Ni, S), Co_8MS_8, and $Fe_4Ni_4MS_8$ (M = Ru, Rh, Pd)*

OSVALD KNOP, CHUNG-HSI HUANG,† K. I. G. REID‡ AND J. S. CARLOW§

Department of Chemistry, Dalhousie University, Halifax, Nova Scotia B3H 4J3, Canada

AND

F. W. D. WOODHAMS

Department of Natural Philosophy, University of Aberdeen, Aberdeen AB9 2UE, Scotland

Received January 20, 1975; in revised form, May 6, 1975

The metal atoms in the cubic π phases (Fe, Co, Ni, $M)_9S_8$ occupy 4-coordinated majority and 6-coordinated minority sites in the ratio 8 : 1. X-ray and neutron powder diffraction of Co_8MS_8 and $Fe_4Ni_4MS_8$ (M = Fe, Co, Ni, Ru, Rh, Pd) has shown that the structures are ordered, i.e., with M segregated in the minority sites, when M is a 4*d* element, and at best partially ordered when M is a 3*d* element. Magnetic susceptibility measurements and Mössbauer ^{57}Fe spectra show that Co_9S_8 and the natural π(Fe, Ni, S) phase, *pentlandite*, remain Pauli-paramagnetic down to 4.2°K, with no resultant magnetic moments on the metal atoms, and hence are broad-band metals. Linear dependence of the isomer shifts at the two types of sites in a variety of (Fe, Co, Ni)$_9S_8$ compositions indicates the existence of a composite *s–d* conduction band. Analysis of the variation of the quadrupole splitting at the majority site with composition leads to the conclusion that only a few levels at the bottom of the conduction band are occupied. The number of electrons in the band is approximately proportional to the total *d*-electron content of the unit cell. A tentative band scheme based on these results and on other available evidence is proposed. The effect of composition on the interatomic distances in the π phases is discussed.

In a previous study (*1*) we established that the Mössbauer ^{57}Fe spectrum of the mineral pentlandite (*P*), (Fe, Ni)$_9S_8$, consists of a dominant symmetric quadrupole doublet and a weak single line, as would be expected from the existence of two types of cation sites in the crystal structure of the mineral. The isomer shift $\delta(f)$ associated with the Fe atom in the tetrahedrally coordinated majority site 32(f) is significantly smaller than the $\delta(b)$ of Fe in the octahedrally coordinated site 4(b), but the general smallness of both isomer shifts as well

* For Part IX, see Ref. *38*. This paper is based in part on the Ph.D. theses submitted to the Department of Chemistry, Dalhousie University, by K. I. G. Reid (*3*) and C.-H. Huang (*4*).

† INCO Graduate Fellow, 1968–1970. Present address: Department of Chemistry, Memorial University of Newfoundland, St. John's, Newfoundland A1C 5S7, Canada.

‡ Present address: Central Research Laboratory, N.L. Industries Inc., Hightstown, N.J. 08520.

§ Killam Postdoctoral Fellow, 1972–1974. Present address: Department of Physics, University of Southampton, Southampton SO9 5NH, England.

as of the quadrupole splitting Δ, instead of providing an answer about the valency and spin states of the two types of Fe atoms, raised further questions. In an attempt to clarify the situation Mössbauer spectra were obtained of synthetic π(Fe, Co, Ni, S), π-Co_8MS_8, and π-$Fe_4Ni_4MS_8$ (M = Ru, Rh, Pd) phases isostructural with P. Some of these preparations had been previously examined (*2–4*) by X-ray and neutron diffraction to determine the nature of the distribution of the metal atoms over the 32(f) and 4(b) lattice complexes. The tendency to preferential occupancy of the octahedral sites which was observed in some of the preparations, seemed to suggest that the combined diffraction and Mössbauer results could be discussed in terms of a localized-electron model. On the other hand, the type π phase Co_9S_8 had been reported to be a metallic conductor (*5*), hence a band model would be required. A further complication arose from the conflicting claims (*6*, *7*) as to the magnitude and temperature dependence of the magnetic susceptibility of Co_9S_8: only the results reported in (*7*) are consistent with metallic behavior. Therefore, measurements of the susceptibility of Co_9S_8 and P down to 4.2°K were undertaken to remove the discrepancy and to determine which of the two models was appropriate.

Experimental

Preparation of Samples[1]

Natural P was extracted from specimens of coarsely crystalline ore from the Creighton mine, Sudbury, Ontario. It was the same material as used in (*1*), i.e., S of (*8*).

Samples *WA*, *WB*, *WC*, *X*, *Y*, and *Z* had been prepared by Sutarno (*2*), who determined their $a_0(\pi)$ values (Table I) and carried out preliminary refinements of their crystal structures from X-ray data with a view to determining the extent of ordering. All the other samples examined by Mössbauer spectroscopy and neutron diffraction were prepared by direct synthesis from high-purity elements (cf. *9*) and subsequently ground and annealed in small, evacuated, and sealed quartz tubes for homogenization. Their annealing schedules are shown in Table I. When homogenized at or above 600°C, the powders in most cases strongly sintered yielding compact slugs that had to be crushed and ground before final annealing below 600°C. The powders were brittle and had metallic appearance. Those containing Pd were bright brass-yellow, those containing Ru or Rh were silvery gray, as were also (Fe, Co, Ni)$_9S_8$ samples rich in Fe. Samples rich in Ni were pale yellow, while massive Co-rich alloys were grayish-white.

Samples G' and I were enriched using metallic iron 91% in ^{57}Fe. The iron content of G' consisted of about 50% and that of I, about 20% ^{57}Fe.

Densities of the sulfide powders were measured by double weighing as described in (*1*).

X-Ray Diffraction

Integrated intensities were obtained with a Philips powder diffractometer, which in the later stages of this investigation was fitted with a focusing monochromator after the rotating specimen. This arrangement gave very low background counts even with unfiltered CuK radiation. For details of specimen preparation, etc., Refs. (*10*) and (*11*) may be consulted. The wavelengths employed were $\lambda(\text{Fe}K\alpha_1) = 1.93604$ Å, $\lambda(\text{Fe}K\bar{\alpha}) = 1.93736$ Å, $\lambda(\text{Cu}K\alpha_1) = 1.54056$ Å, and $\lambda(\text{Cu}K\bar{\alpha}) = 1.54184$ Å.

X-ray scattering factors for neutral atoms (see *12* for the metals, *13* for sulfur) and dispersion corrections (both parts, *14*) were used in ad hoc full-matrix least-squares refinements. Weighting scheme W3 (cf. *15*) was normally employed in refinements from $|F_0|$, while in refinements from intensities the weights were defined as $w(hkl) = \varepsilon^{-1}(hkl)$ (weighting scheme W4).

Neutron Powder Diffraction

The neutron diffraction experiments were performed at the NRX reactor of Atomic Energy of Canada Ltd. at Chalk River,

[1] For the sake of brevity π-phase compositions will be referred to as isoelectronic if they contain the same number n_d of $3d$, or $3d+4d$, electrons per formula unit. Compositions with $n_d = 63$ are termed electron-precise or eu-electronic, those with $n_d < 63$ hypoelectronic, and those with $n_d > 63$, hyperelectronic.

TABLE I

PREPARATION, DENSITIES, AND LATTICE PARAMETERS OF SYNTHETIC π PHASES[a]

Sample	Gross composition	Heat treatment after reaction	$a_0(\pi)$ (Å)
H	Co_9S_8	600/2d, 500/18h → 1d → R.T.	9.9273(4)
G′	$Co_{8.82}{}^{57}Fe_{0.18}S_8$	700/4d, 650/4d, 600/2d, 450/1d	
A	Co_8FeS_8	650/1d, 600/1d, 550/10d, 500/25d	9.941(1)
A′	Co_8FeS_8	600/5d, 550/25d, 500/6d; $d_e = 5.224(9)$, $d_x = 5.294$	9.944(1)
A″	Co_8FeS_8	700/6d → 34h → 500/2d → 3d → R.T.	9.945(3)
I	$Co_8{}^{57}Fe_{0.5}Ni_{0.5}S_8$	650/3h, 600/1d, 550/6d, 500/7d	9.942(1)
M	Co_8NiS_8	570/2d, 540/15d, 500/30d; $d_e = 5.247(7)$, $d_x = 5.316$	9.942(1)
L	$Co_7Fe_2S_8$	650/1d, 600/2d, 550/12d, 500/2d; π + T	9.951(1)
B	Co_7FeNiS_8	650/1d, 550/2d, 500/25d	9.952(1)
C	$Co_6FeNi_2S_8$	650/1d, 600/3d, 550/2d, 500/25d	9.967(1)
D	$Co_5FeNi_3S_8$	650/1d, 600/3d, 550/2d, 500/25d	9.983(1)
N	$Co_4Fe_2Ni_3S_8$	650/1d, 600/2d, 550/11d, 500/2d; π + T	9.995(1)
E	$Co_4FeNi_4S_8$	600/3d, 550/4d, 500/15d; $d_e = 5.149(7)$, $d_x = 5.199$	10.000(1)
J	$Co_3Fe_3Ni_3S_8$	650/1d, 600/3d, 500/18d; π + Po	10.010(1)
F	$Co_3FeNi_5S_8$	650/1d, 550/5d, 500/18d; π + M	10.021(1)
K	$CoFe_4Ni_4S_8$	570/2d, 540/15d, 500/4d; $d_e = 4.984(6)$, $d_x = 5.037$	10.067(1)
R	$Fe_5Ni_4S_8$	600/2d, 550/3d, 500/15d; $d_e = 4.880(6)$, $d_x = 4.926$	10.128(1)
S	$Fe_{4.5}Ni_{4.5}S_8$	600/4d, 550/4d, 500/1d; $d_e = 4.896(10)$, $d_x = 4.964$	10.109(1)
U	$Fe_4Ni_5S_8$	560/1d, 500/24d; $d_e = 4.957(2)$, $d_x = 4.986$	10.100(1)
V	$Fe_{3.5}Ni_{5.5}S_8$	600/4d, 550/6d, 500/3d	10.094(2)
WA	Co_8RuS_8	700/3d, 600/3d → 6d → R.T.; π + RuS_2(tr)	9.944(1)
WB	Co_8RhS_8	700/3d (signs of incipient melting), 600/4d → 4d → R.T.	9.977(1)
WC	Co_8PdS_8	700/3d (very strong sinter, single crystals appearing at surface of slug), 600/3d → 5d → R.T.; see text	10.008(1)
Y	$Fe_4Ni_4RuS_8$	700/9d, 700/2d, 600/3d, 600/6d, 750/1d → 7d → R.T.; π + Po? (tr)	10.046(1)
X	$Fe_4Ni_4RhS_8$	700/4d, 600/4d → 4d → R.T.; π + Po(tr)	10.087(1)
Z	$Fe_4Ni_4PdS_8$	700/4d (sample melted?), 600/5d → 5d → R.T. (very strong sinter), 350/10d, cooled with furnace; see text	10.216(2)

[a] 600/2d stands for 600°C for 2 days; 500/18h → 1d → R.T. stands for 500°C for 18 hr, then controlled cooling in the furnace over 1 day to room temperature. In most cases only the last sequence of heat treatment is indicated. d_e, d_x: experimental and calculated densities, g/cm³. T, troilite; Po, pyrrhotite; M, millerite.

Ontario. The neutron beam was monochromatized by reflection from the 111 plane of either an Al ($2\theta_M = 40°$, $\lambda = 1.600$ Å) or a squeezed Ge ($2\theta_M = 32°$, $\lambda = 1.801$ Å) crystal. A single-crystal quartz filter 6 in. thick reduced the second-order (Al) and third-order (Ge) contents of the incident beam to less than 1 %. The raw diffraction patterns were reduced to pF^2 patterns, and overlapping peaks were resolved and Gaussian profiles were fitted to all the peaks by least squares.

The neutron scattering amplitudes b(Fe) = 0.96, b(Co) = 0.25, b(Ni) = 1.03, b(S) = 0.31 (all in 10^{-12} cm), and ad hoc full-matrix programs were used in the least-squares refinements.

Mössbauer ^{57}Fe Spectra

The apparatus and technique have been described in (*1*). In running the spectra of *P* above room temperature the sample (*in vacuo*) was kept at the temperature selected for at least 6 hr before starting to accumulate the spectrum. As in (*1*), the spectra were fitted to either (*a*) two independent single lines or (*b*)

a single line superposed on a symmetric quadrupole doublet. These fits will be referred to in the following as models *a* and *b*, respectively. For a statistically acceptable fit χ^2 was required to lie between the 1 and 99% limits of the χ^2 distribution, i.e., between about 150 and 242 for spectra with 194 degrees of freedom. $\delta(f)$ and $\delta(b)$ designate the isomer shifts at the 32(f) and 4(b) sites respectively; Δ is the quadrupole splitting of the spectrum corresponding to 32(f). The isomer shifts are quoted relative to metallic Fe at room temperature.

Magnetic Susceptibility

The susceptibilities of Co_9S_8 and two samples of natural *P* were measured at temperatures between 4.2 and 300°K by the Faraday method. The samples were allowed to come to thermal equilibrium at each temperature before readings were taken. Temperature control was accurate to ±0.3°K; temperatures were measured with calibrated copper–constantan thermocouples.

The *P* samples could not be freed from ferromagnetic impurity even by repeated crushing, hand-picking, magnetic separation, and further hand-picking under the microscope. Since the impurity contributed about 40% to the measured susceptibility in each of the two samples, the field required to saturate the impurity was determined from plots at 4.2 and 300°K and a correction applied as follows.

The force F on the sample is given by $F = (\chi/\rho)\,(m/\mu_0)\,B(dB/dz) + M_s \int (dB/dz)dv$, where m = mass of sample, χ/ρ = susceptibility in m^3/kg, μ_0 = permittivity of free space, $B(dB/dz)$ = product of the magnetic field and the field gradient of the sample, M_s = magnetization of the ferromagnetic impurity assumed saturated, and v = impurity volume. In the Faraday method, measurements are carried out with the sample in a region of constant $B(dB/dz)$; in the apparatus used this term was constant to ±0.2% over the sample length of 1.0 cm. This may be expressed as $B(dB/dz) = H(I)$, where H is some function depending only on the properties of the magnet and its current I. Integrating we obtain $B^2 = 2H(I)\,(z + z_0)$, whence $dB/dz = [H(I)\ /\ 2(z + z_0)]^{1/2}$. The equation for F then becomes

$$F = (\chi/\rho)\,(m/\mu_0)\,H(I) + M_s H(I)^{1/2} \times \int [2(z + z_0)]^{-1/2}\,dv = pH(I) + qH(I)^{1/2}.$$

At all sample temperatures force measurements (corrected for contribution from the sample container) were recorded at two different magnet currents to allow evaluation of p and q. The value of $H(I)$ for a given I was obtained by calibration with a Pd reference sample. The susceptibility of *P* was deduced from the value of p, while q was monitored throughout the temperature range for any increase which could be ascribed to a magnetic transition in *P* or the impurity.

Results

Lattice Parameters of the π Phases

The lattice parameter of Co_9S_8 (Table I) agreed well with most of the recent literature values (*2*, *7*, *9*, *16–18*) except with the value 9.917 Å in (*19*).

Of the compositions containing 4*d* elements only *WB* was homogeneous, within the limits of detection by careful X-ray powder diffraction. The amounts ("traces") of foreign phases present in the other preparations were small. The exception was *WC* and *Z*, in which the inhomogeneity was significant; on annealing, their powders were strongly sintered at temperatures at which the Ru- and Rh-containing sulfides would be free-flowing. The principal secondary phase was PdS (cf. also *20*). The exact compositions of $\pi(WC)$ and $\pi(Z)$ were thus not known. The pronounced cleavage and crystallinity of *WC* and *Z* tended to affect adversely the results of powder photography and diffractometry through preferred orientation. Similar difficulties had been experienced elsewhere (*2*, *20*).

In the π(Fe, Co, Ni, S) phases the gradient of $a_0(\pi)$ is roughly along the eu-electronic join Co_9S_8–$Fe_{4.5}Ni_{4.5}S_8$ of the M_9S_8 section of the system Fe–Co–Ni–S (line *H*, *I*, *B*, *J*, *K*, *S* in Fig. 1a; cf. *9*). In comparison, the variation produced by changes in the Fe : Ni ratio at constant Co is relatively small except in the low Co range (Fig. 1a): the total change in

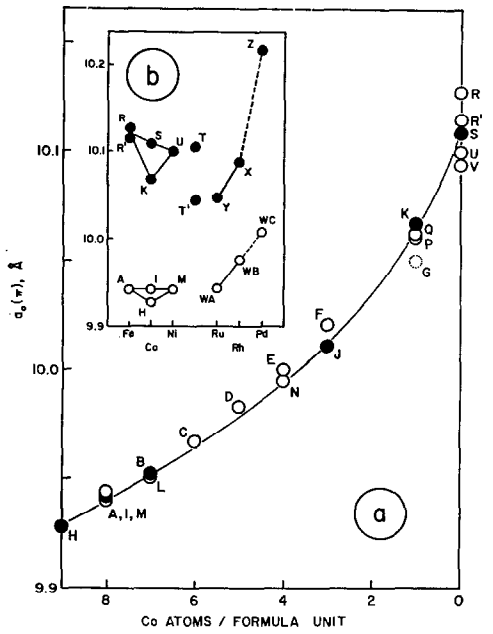

FIG. 1. Dependence of the lattice parameter $a_0(\pi)$ on composition. (a) Variation with the number of Co atoms per formula unit (Fe, Co, Ni)$_9$S$_8$. Full circles, eu-electronic compositions, $n_d = 63$; open circles, hypo- or hyperelectronic compositions (n_d values are shown). Compositions not shown in Table I: *G*, "CoFeNi$_7$S$_8$"; *P*, CoFe$_2$Ni$_6$S$_8$; *Q*, CoFe$_3$Ni$_5$S$_8$. (b) Variation with *M* for compositions Co$_8M$S$_8$ (open circles) and Fe$_4$Ni$_4M$S$_8$ (full circles), *M* = Fe, Co, Ni, Ru, Rh, Pd. Points for pentlandite (*T*, *T'*) are also shown.

$a_0(\pi)$ over the *entire* π(Fe, Ni, S) range is ~0.135 Å (*9*, *21*) as against ~0.18 Å from *H* to *S*. In the absence of Co $a_0(\pi)$ increases steeply with the Fe : Ni ratio and thus with the increasing population of 32(*f*) by Fe atoms.

The $a_0(\pi)$ values for *WA*, *WB*, and *WC* were practically the same as reported previously (*20*). The variation of $a_0(\pi)$ with *M* in Co$_8M$S$_8$ and Fe$_4$Ni$_4M$S$_8$ is shown in Fig. 1b.

The measured densities (Table I) were always slightly lower than the X-ray densities. The difference, 0.6(1) to 1.5(2)%, is in the natural direction of experimental error, but some of it may be attributed to slight admixtures of troilite or pyrrhotite not detected by powder photography.

Refinement of the Structure of Co$_9$S$_8$

There was no significant difference between the results of *F*-refinements using *B*(overall) and *B*(individual isotropic) (Table II), and the agreement of I_0 with I_c calculated from the final parameter values was very satisfactory. Geller's (*16*) parameter values obtained with a single crystal[2] agree with ours to within twice the stated σ limits, but the present *B*(S) values are always positive definite and in the range expected. Geller's $\sigma(K)$ are significantly larger than ours, which may be indicative of uncertainties in the scale factor correlating intensities measured in different Weissenberg films, a source of difficulty absent in powder diffractometry. All our parameter values are very close to those obtained by Rajamani and Prewitt (*22*) from a single crystal of Co-rich Outokumpu pentlandite, Fe$_{1.63}$Ni$_{1.82}$Co$_{5.60}$S$_8$ (Table II).

Refinement of the Structures of the Mixed π Phases

The degree of occupancy of 4(*b*) by *M* in mixed π phases A$_8M$S$_8$ is defined by an ordering parameter *s* which must be included as a parameter of refinement: $f(4b) = (1-s)f_A + sf_M$ and $f(32f) = [(7+s)f_A + (1-s)f_M]/8$, and similarly for the neutron scattering amplitudes b_A and b_M.

X-ray diffraction. The Co$_8M$S$_8$ and Fe$_4$Ni$_4M$S$_8$ phases were refined for *K*, *x*, *u*(S), *B*(overall), and *s* (or at fixed *s*) from $|F_0|$'s extracted from powder diffractometer intensities (Fe*K*α). Despite the substantial differences between the scattering factors of the 3*d* and the 4*d* atoms the uncertainties of the refined values of *s* were large (Fig. 2); nevertheless, the respective $\sigma(s)$ ranges for *WA*, *WB*, *X*, and *Y* included $s = 1$, and so the tendency of the 4*d* atoms to occupy 4(*b*) sites is demonstrated (cf. also *2* and *20* and the single-crystal refinement of argentian pentlandite, *23*). A similar conclusion applies to *WC* and *Z*, even though the intended compositions assumed in the refinement are not quite correct. The other parameter values also

[2] Visual intensities were estimated from Weissenberg *hk*0 and *hk*1 levels. The smallness of Geller's *B*(S) values is the subject of his own comment.

TABLE II

F-REFINEMENTS OF THE CRYSTAL STRUCTURE OF Co_9S_8 FROM X-RAY DATA[a]

Parameter		Ref. (*16*)	Present work[b]		Ref. (*22*)[c]
Number of $\|F_o\|$		56 (Mo$K\alpha$)	25 (Fe$K\alpha$)[d]		95 (Mo$K\alpha$)
K	(*hk*0)	1.038(17)	0.964(9)	0.977(6)	
	(*hk*1)	0.960(23)			
x(Co)		0.1260(3)	0.1266(3)	0.1266(3)	0.12617(2)
u(S)		0.2591(11)	0.2624(9)	0.2620(8)	0.2623(1)
B(32*f*), Å^2		0.39(3)	0.55(7)	—	0.49(2)
B(4*b*), Å^2 (*m*3*m*)		0.55(21)	0.67(23)	—	0.55(3)
B(24*e*), Å^2		0.17(11)	0.60(12)	—	0.49(2)
B(8*c*), Å^2 ($\bar{4}3m$)		0.07(25)	0.53(25)	—	0.621(3)
B(overall), Å^2		—	—	0.63(4)	—
R, %		?	1.76[d]	1.89[d]	1.8[e]

[a] Space group *Fm*3*m*; Co in 4(*b*) and 32(*f*), S in 8(*c*) and 24(*e*).

[b] Weighting scheme W3.

[c] Co-rich *P* of composition $Fe_{1.63}Co_{5.60}Ni_{1.82}S_8$ from Outokumpu, Finland.

[d] This accounts for all single peaks possible up to 933 + 771 + 755.

[e] Anisotropic temperature factors.

had large standard deviations and, with the exception of u(S), did not show detectable dependence on composition. The average of the x values was 0.126(3) and of the B(overall) values, 0.55(30) Å^2. The $d_{be} = a_0(\frac{1}{2} - u)$ distances calculated from the u(S) values are presented in Fig. 15.

The final value of x for untreated *P* was 0.1267 (5), no matter whether four- or seven-parameter refinements from 28 $|F_o|$ (weighting scheme W3) or from 43 I_o (weighting scheme W4) were used, always assuming Fe + Ni to be distributed at random. By contrast, u(S) refined to slightly different values depending on the type of refinement, the best estimate being 0.2633(15). The R values were not as good for *P* as for Co_9S_8, about 5% for the *F*-refinements and about 9% for the *I*-refinements, even though the specimens were prepared and the intensities (Cu$K\alpha$) collected with no less care. These best estimates of x and u are in very good agreement with the recent single-crystal refinements of natural *P* by Rajamani and Prewitt (*22*) and by Hall and Stewart (*23*): $x = 0.12608(4)$, $u = 0.2632(1)$ for Frood mine *P* (*22*), and $x = 0.1261(1)$, $u = 0.2629(2)$ for a Sudbury *P* of unspecified origin (*23*).

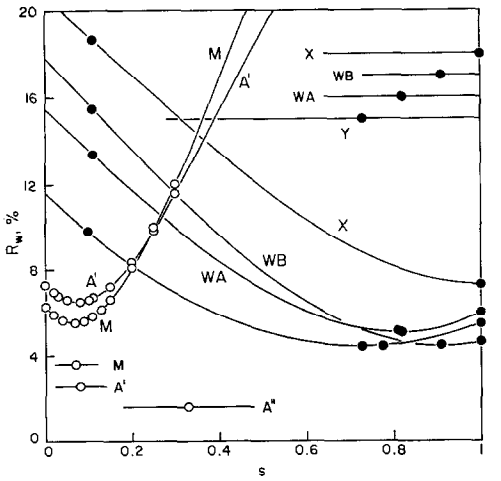

FIG. 2. Variation of the discrepancy index R_w (in %) with the ordering parameter s for refinements from X-ray diffraction (*WA*, *WB*, *X*, *Y*; full circles) and neutron diffraction (*A'*, *A"*, *M*; open circles) data. The 1σ limits of the final values of s are indicated by horizontal bars.

Neutron diffraction. The number of reflections in the neutron powder patterns (Fig. 3) was even smaller than in the X-ray patterns. This and the Gaussian analysis of the diffraction peaks, together with the somewhat arbitrary choice of baseline in the reduced (pF_0^2) patterns, introduced further uncertainties into the refinements. There was also some uncertainty as to what are the best values of b(Co) and b(S) (cf. *10*).

Strictly speaking, only ternary $(A, A')_9S_8$ π phases can be refined using the ordering parameter s. For $Fe_5Ni_4S_8$ (R) and $Fe_4Ni_5S_8$ (U) the s-refinements led to inconclusive results: b(Fe) and b(Ni) differ by only about 7%, i.e., about as much as the X-ray scattering factors. In view of this, it seemed reasonable to estimate the Co populations of the 4(b) sites in E and K by refining for s, i.e., making no distinction between Fe and Ni.

The several refinements involving different numbers of parameters that were tried for samples A', M, E, and K turned out to be relatively insensitive to the particular assumptions made. A plot of R_w for a K, x, u, B(overall) refinement at fixed s against s (Fig. 2) shows that the metal atoms in both A' and M were distributed at random. This result for M agrees with a previous conclusion based on less complete evidence (*9*). However,

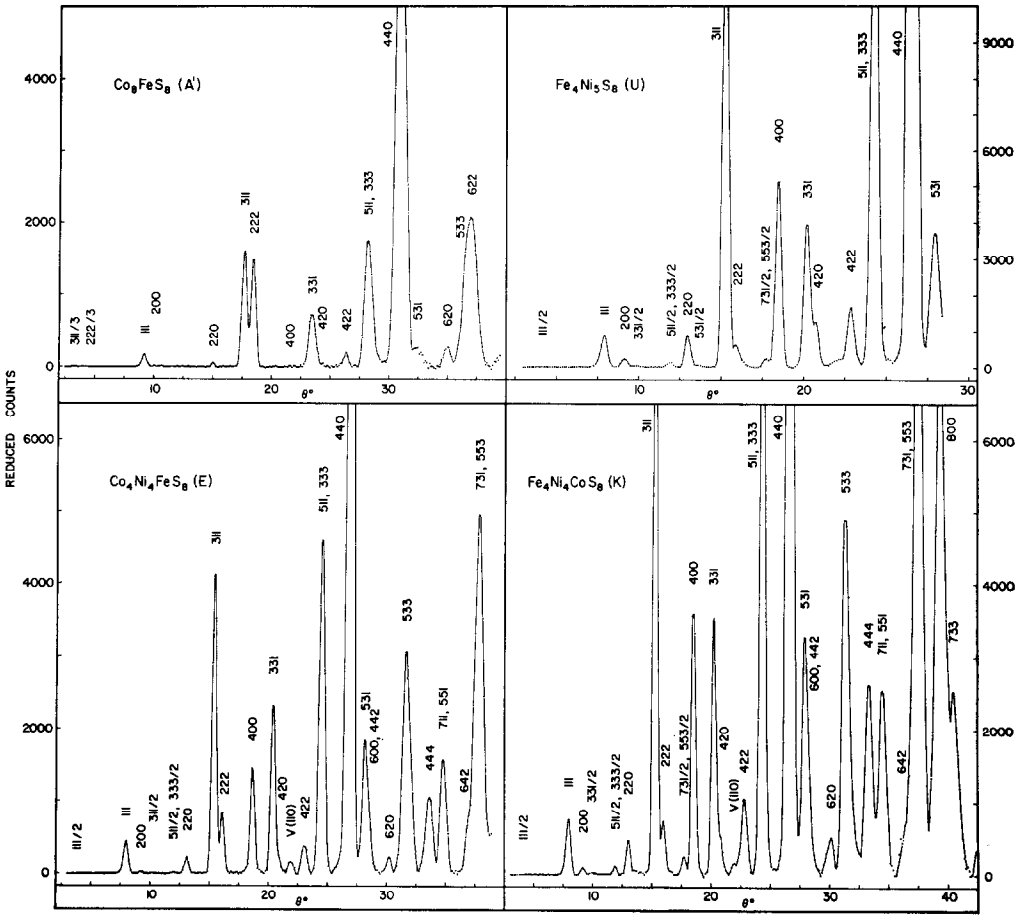

FIG. 3. Typical reduced (pF^2) neutron diffraction patterns at room temperature. Monochromator, Ge(111) for A' (about 16 min per point), Al(111) for U (about 16 min per point), E and K (about 18 min per point). V(110), spurious peak from vanadium foil containing the sample powder.

in another Co_8FeS_8 sample, A'', there appeared to be some tendency to ordering. The discrepancy may be attributable to the different thermal histories of A' and A''. By contrast, refinements of E indicated 0.66(16) Co atoms per 4(*b*) site ($R = 4.1\%$) compared with 0.445 for a statistical distribution ($R = 9.8\%$). In K the degree of occupancy of the octahedral site by Co was even greater, 0.35(10) Co per site ($R = 4.9\%$) as against 0.11 for a random distribution ($R = 8.1\%$).

Considering the appreciable differences in the appearance of the neutron diffraction patterns (Fig. 3), the results of these refinements are not as conclusive as one might think they ought to be. However, they are the best that could be obtained in circumstances that are on the whole unfavourable to good refinement.

Interatomic Distances

In Co_9S_8 the present M–S distances (in Ångstroms, uncorrected for thermal motion) agree with Geller's (*16*) to within 3σ and are consistent with the corresponding distances in the 4*d* phases and in the Co-rich Outokumpu *P* of (*22*):

	This work[3]	*Geller*[3]
Co(*f*)–S(*c*)=d_{fc}	2.122(15)	2.132(15)
Co(*f*)–S(*e*)=d_{fe}	2.231(22)	2.208(24)
Co(*b*)–S(*e*)=d_{be}	2.361(27)	2.392(33)
Co(*b*)–S(*c*)=d_{bc}	4.299(1)	4.299(1)
Co(*f*)–Co(*f*): $d_1=2a_0x$	2.514(18)	2.501(18)
$d_2=(\frac{1}{2}a_0-d_1)\sqrt{2}$	3.465(26)	3.481(24)
$d_3=d_1\sqrt{2}$	3.555(26)	3.538(26)
Co(*f*)–Co(*b*)=$d_4=a_0(3x^2-x+\frac{1}{4})^{1/2}$	4.111(2)	4.113(2)

The Co–Co distances relative to a central Co(*f*) atom are shown in Fig. 4.

The weighted average Co(*f*)–S in the $Co^fS_1{}^cS_3{}^e$ tetrahedron is 2.20 Å, i.e., not distinguishable from the Co^{iv}–S distance in

[3] The σ values of (*16*) have been multiplied by three and additional distances have been calculated from Geller's parameter values.

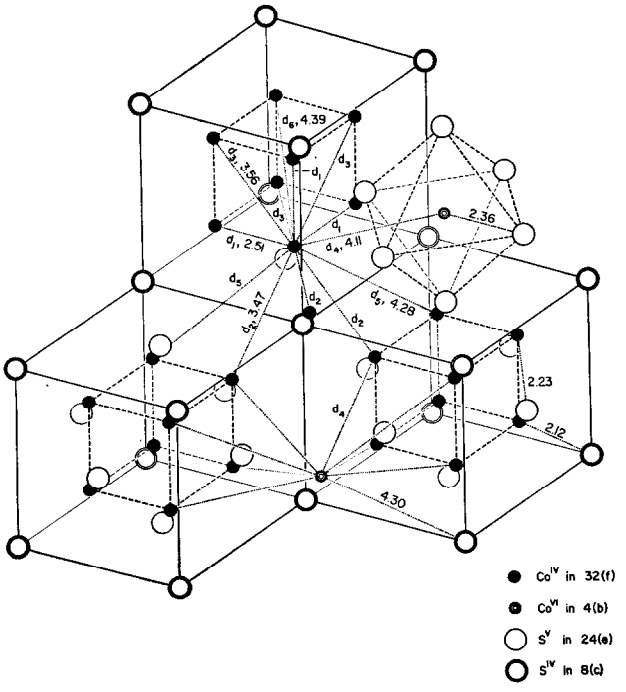

FIG. 4. View of a portion of the Co_9S_8 structure showing the coordinations of the Co(*b*), Co(*f*), and S(*e*) atoms and the Co–Co distances d_1 to d_6 (see text; $d_5 = (12x^2 - 4x + \frac{1}{2})^{1/2}a_0$, $d_6 = d_1\sqrt{3}$).

TABLE III

DEPENDENCE OF THE MÖSSBAUER PARAMETERS (IN MM/SEC) OF A PENTLANDITE SPECIMEN ON ITS THERMAL HISTORY[a]

	Quadrupole spectrum			Single-line spectrum			
T(°C)	$\delta(f)$	$\lvert\Delta\rvert$	$\Gamma(f)$	$\delta(b)$	$\Gamma(b)$	r^b	χ^2
R.T.[c]	0.355(4)	0.320(6)	0.312(9)	0.650(8)	0.31(3)	4.6(5)	245, 215
140	0.276(8)	0.243(9)	0.29(2)	0.565(14)	0.33(3)	2.9(8)	173, 172
200	0.253(12)	0.202(24)	0.28(3)	0.46(5)	0.41(14)	4(2)	194, n.c.
300	0.228(12)	0.18(2)	0.28(2)	0.51(8)	0.37(16)	11(4)	245, 240
100	0.333(5)	0.267(12)	0.289(14)	0.667(16)	0.34(4)	8(3)	131, 168
R.T.[d]	0.364(4)	0.305(8)	0.276(11)	0.662(18)	0.23(5)	10(2)	205, 186

[a] Isomer shifts relative to metallic Fe at room temperature. The pairs of χ^2 values are for mirror-image spectra; n.c., not converged.

[b] Area ratio $r = \mathrm{Fe}(f):\mathrm{Fe}(b)$.

[c] Sample T' of Table I.

[d] Sample T of Table I.

the spinel Co_3S_4, 2.18(5) Å (*24*). The d_{be} distance in the regular $Co^bS_6{}^e$ octahedron is about the same as the Co^{iv}–S distance in the pyrite CoS_2, 2.323(3) Å (*3*), but it is significantly larger than the Co^{vi}–S distance in the spinels Co_3S_4, 2.271(24) Å, and $Ni[Co_2]S_4$, 2.27(1) Å (*24*).

The very short distance d_1 is the edge length of the $Co_8{}^f$ cubes present in the antifluorite cubic subcells of the π structure. It is the same as the shortest Co–Co distance in metallic Co (C.N. 12), but much shorter than the Co^{vi}–Co^{vi} distance in CoS_2, 3.91 Å, or the metal–metal distances in Co_3S_4: Co^{iv}–Co^{iv}, 4.07 Å, Co^{vi}–Co^{vi}, 3.33 Å, and Co^{iv}–Co^{vi}, 3.90 Å.

Mössbauer Spectra of Natural Pentlandite

Spectra taken between room temperature and 300°C were fitted to model *b*. They confirm our previous results (Table III). By 300°C, $|\Delta|$ has decreased sufficiently for the single line originating at 4(*b*) to be clearly visible (Fig. 5a). The change in the area ratio r of the doublet to the single line illustrates beyond doubt the redistribution of Fe atoms between 4(*b*) and 32(*f*) that gives rise to the irreversible expansion of the unit cell discussed in (*1*). The effect of the redistribution is also visible in the temperature variation of the isomer shifts on heating and on cooling (Fig. 6).

A spectrum obtained at 15°K in an external magnetic field of 45 kOe parallel to the γ-ray

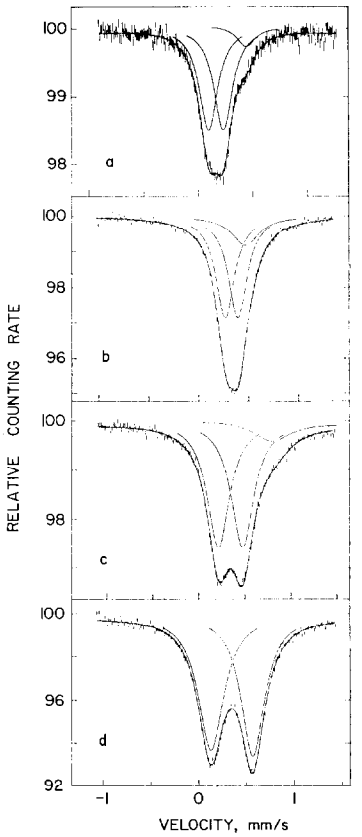

FIG. 5. Mössbauer ^{57}Fe spectra. (a) Pentlandite at 300°C; (b) Co_8FeS_8 (*A*); (c) $Co_8^{57}Fe_{0.5}Ni_{0.5}S_8$ (*I*); (d) $Fe_4Ni_4RhS_8$ (*X*) (the last three at room temperature). The solid curves are computer fits to model *b* (see text).

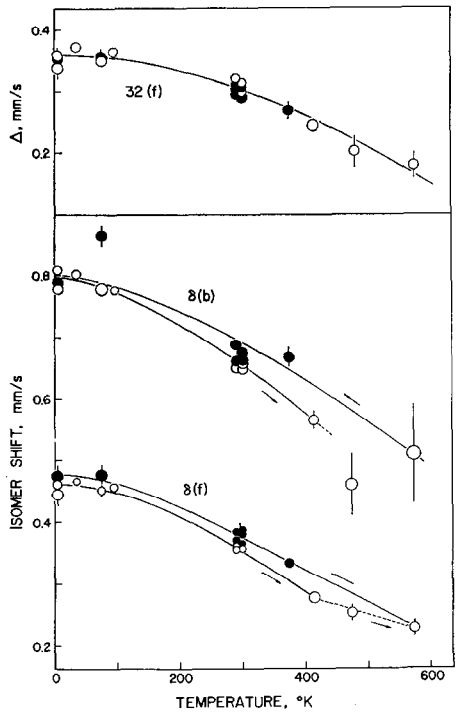

FIG. 6. Temperature dependence of $\delta(f)$, $\delta(b)$, and $|\Delta|$ for natural pentlandite (combined results of Table III and (*1*)). Open circles, untreated material. Full circles, after annealing at ≥200°C.

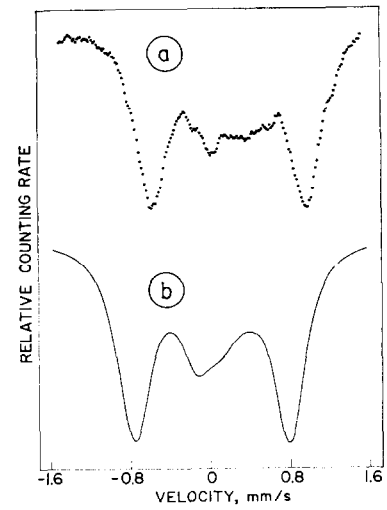

FIG. 7. Mössbauer ^{57}Fe spectra of pentlandite. (a) Untreated material at 15°K in an external field of 45 kOe parallel to the γ-ray beam (spectrum smoothed by carrying out a five-channel moving average). (b) Simulated spectrum with parameters $H = 45$ kOe, $(\frac{1}{4}e^2qQ)_f = 0.36$ mm/sec, $\eta = 0$, $(\frac{1}{4}e^2qQ)_b = 0$, $\delta(b) - \delta(f) = 0.3$ mm/sec, $\Gamma = 0.3$ mm/sec, $r = \text{Fe}(f):\text{Fe}(b) = 4.5$.

direction showed clear evidence of four lines (Fig. 7a).[4] Theoretical spectra were computed for comparison using a simulation program (*26*) appropriate to the case of a fixed orientation between the electric field gradient (EFG) and the crystallographic axes, and taking into account that in a powder specimen all angles between the external magnetic field H_{ext} and the EFG are possible. Values of e^2qQ, isomer shifts and line widths appropriate to 32(f) and 4(b) in P at 15°K were used. The Fe(f):Fe(b) = r ratio was taken as 4.5, the value for natural P. Spectra were simulated for a wide range of combinations of magnetic fields H at the two sites. It was found, however, that the experimental spectrum was best reproduced with $H = 45$ kOe at both sites, $\eta = 0$, and $e^2qQ < 0$ (Fig. 7b). There is thus no evidence of any measurable hyperfine magnetic field at either site. Any field at 4(b) greater than about 70 kOe would have shown up clearly as structure on the high-velocity wings of the spectrum.

[4] A similar spectrum of P, in an external magnetic field of 30 kOe at 4.2°K, has been reported by Vaughan and Ridout (*25*).

Mössbauer Spectra of Synthetic π Phases

Spectra of the 3d π phases (Table IV) were very similar in appearance to that of annealed P (Fig. 1 of *1*), showing an asymmetric doublet with a small splitting. Exceptions were two of the three compositions containing no Ni, Co_8FeS_8 (A) and $Co_7Fe_2S_8$ (L), whose spectra showed only a slightly broadened single line. A long-run spectrum of A (Fig. 5b) showed that the shape of this single line was not Lorentzian: a one-line fit gave statistically unacceptable χ^2 values of 799 and 482 for the two mirror-image spectra accumulated. These χ^2 values were substantially reduced when the spectrum was fitted to either model a (242, 238) or model b (241, 212). Although statistically both fits are acceptable, a gave area and linewidth ratios for the low-to-high velocity line

TABLE IV

MÖSSBAUER ^{57}Fe PARAMETERS (IN MM/SEC) OF SYNTHETIC π PHASES[a]

Sample	T(°K)	Quadrupole spectrum			Single-line spectrum		r
		δ(f)	|Δ|	Γ(f)	δ(b)	Γ(b)	
G′	R.T.	0.337(2)	0.212(4)	0.241(6)	0.72(4)	0.64(10)	5(1)
A	R.T.	0.340(6)	0.125(6)	0.231(10)	0.48(4)	0.35(8)	6(3)
I	R.T.	0.339(10)	0.260(6)	0.297(8)	0.74(6)	0.45(10)	8(2)
	77	0.435(4)	0.279(6)	0.324(14)	0.91(6)	0.51(14)	9(4)
L	R.T.	0.348(22)[b]	0.10(2)[b]	0.26(3)[b]			
B	R.T.	0.338(7)	0.268(10)	0.27(2)	0.62(16)	0.5(3)	8(5)
C	R.T.	0.32(4)	0.328(12)	0.286(16)	0.60(3)	0.20(6)	12(4)
D	R.T.	0.312(4)	0.357(8)	0.267(12)	0.592(14)	0.20(5)	8(2)
N	R.T.	0.327(6)	0.349(12)	0.278(16)	0.56(8)	0.5(2)	5(2)
E	573	0.153(4)	0.320(8)	0.270(12)	0.43(1)	0.24(4)	5.7(8)
	R.T.	0.315(2)	0.398(4)	0.27(1)	0.597(7)	0.24(2)	6.5(6)
	77	0.404(10)	0.412(20)	0.270(18)	0.69(6)	0.24(10)	7(3)
J	R.T.	0.333(2)	0.337(4)	0.291(3)	0.621(5)	0.24(1)	14(1)
	77	0.425(2)	0.359(4)	0.370(4)	0.735(5)	0.18(2)	20(3)
F	R.T.	0.304(3)	0.428(6)	0.252(6)	0.596(8)	0.23(2)	6.4(5)
K	R.T.	0.355(4)	0.302(4)	0.283(6)	0.614(16)	0.30(6)	12(2)
R	R.T.	0.377(4)	0.211(6)	0.265(8)	0.65(2)	0.33(4)	8(1)
S	R.T.	0.367(4)	0.298(4)	0.308(6)	0.685(12)	0.28(4)	12(2)
U	R.T.	0.353(4)	0.322(6)	0.272(8)	0.61(2)	0.30(6)	9(2)
V	R.T.	0.336(2)	0.365(4)	0.271(6)	0.623(12)	0.32(4)	7.1(8)
Y	R.T.	0.361(4)	0.348(4)	0.324(10)[c] 0.311(14)[e]			0.92(10)[d]
X	R.T.	0.353(2)	0.442(4)	0.332(8)[c] 0.306(6)[e]			1.03(6)[d]
	80	0.452(2)	0.485(4)	0.313(10)[c] 0.350(14)[e]			1.10(4)[d]
Z	R.T.	0.374(4)	0.310(4)	0.296(14)[c] 0.248(12)[e]			1.13(10)[d]

[a] Isomer shifts relative to metallic Fe at room temperature. Area ratio $r = \text{Fe}(f):\text{Fe}(b)$.
[b] Single quadrupole-spectrum fit assuming equal-area and width lines.
[c] Two-line fit (model *a*), low-velocity line.
[d] Area ratio of the low- to high-velocity line.
[e] Two-line fit (model *a*), high-velocity line.

of 0.45(8) and 0.75(5), respectively, whereas a third, more realistic quadrupole-doublet model in which areas and line-widths were constrained equal, gave once again unacceptable χ^2 values of 338 and 283. Thus we believe model *b* to be the correct one to use, the statistical analysis of the spectrum giving evidence for Fe occupancy of 4(*b*). Furthermore, the partially resolved asymmetric doublet which constituted the spectrum of the third, enriched π(Fe, Co, S) sample *G′* also was best fitted by *b*. In this case, the line width of the single line was appreciable, 0.64(10) mm/sec, and might be interpreted as evidence of an unresolved doublet at 4(*b*).

Of the 3*d* compositions containing Ni all but *I* and *S* were adequately fitted, unlike *P*, by model *a*; only a small reduction in χ^2 was obtained when model *b* was tried. However, the spectra of *I* (Fig. 5c) and *S*, which resembled that of *P* at 300°C (Fig. 5a), offered direct evidence for the validity of model *b*.

In these two samples the difference between $\delta(f)$ and $\delta(b)$ was sufficiently large for the single line to be visible as a shoulder on the high-velocity component of the quadrupole doublet. Reflecting this the χ^2 values for *I* and *S* were more than 100 lower for *b* than those for *a*, and the area and line-width ratios of the low-to-high velocity lines in all the spectra were noticeably and consistently less than unity. The acceptable χ^2 values obtained with *a* must thus be regarded as fortuitous.

The 4*d* phases, on the other hand, showed symmetric quadrupole spectra and were well fitted by model *a*, which gave equal intensities and line widths for the two lines within experimental error (Table IV). This is consistent with the conclusion from X-ray refinements that in the 4*d* phases the 4(*b*) sites are occupied by 4*d* atoms.

The accuracy of the area ratios *r* (Table IV) for the 3*d* phases is not high enough to aid in the determination of preferential occupancy of 4(*b*) by Fe.

Magnetic Susceptibility

The results for Co_9S_8 and untreated *P* between 4.2 and 300°K are shown in Fig. 8. The susceptibility of Co_9S_8 showed zero field dependence and was almost independent of temperature. The χ–*T* curve was parallel to that reported for the range 80 to 300°K by Townsend et al. (*27*), but our χ values were consistently higher, about 1.4×10^{-6} compared to about 0.5×10^{-6} emu/g. They were also somewhat higher than the value reported for 300°K by Heidelberg et al. (*7*), 1.0×10^{-6} emu/g.[5]

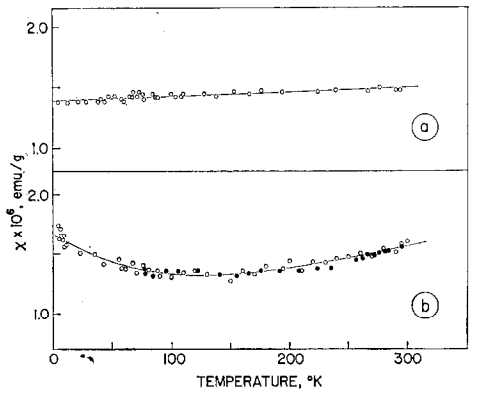

FIG. 8. Temperature dependence of the magnetic susceptibility of (a) Co_9S_8 and (b) untreated natural pentlandite (after correction for ferromagnetic impurity, see text).

Between 80 and 300°K our χ–*T* curve for untreated *P* does not differ greatly from the straight line drawn in this temperature interval by Townsend et al. However, extension to 4.2°K reveals a curvature and an increase in χ with decreasing *T* below about 80°K. The correction term *q* did not show a discontinuity, hence the curvature of the χ–*T* curve cannot be attributed to a transition in the sample.

The smallness of the χ values and their essential independence of temperature down to 4.2°K are indicative of Pauli paramagnetism in both Co_9S_8 and untreated *P*, as already concluded by Townsend et al. from their measurements down to 80°K.

Discussion

Co_9S_8 and Pentlandite

In (*1*), it was shown that in natural *P* the ground states of the Fe(f) and Fe(b) atoms could not be ascertained unambiguously on the Mössbauer evidence then available. Both isomer shifts are small, but they are considerably larger than those of Fe–Ni alloys. The $\delta(b)$ value falls between those for octahedrally coordinated high-spin Fe^{2+} in FeS and low-spin Fe^{2+} in pyrite, although much closer to the former, while $\delta(f)$ lies between the isomer shifts for tetrahedrally coordinated Fe^{3+} in $NaFeS_2$ and Fe^{2+} in $FeCr_2S_4$.

The most important new evidence for the understanding of the nature and physical

[5] The present χ results for Co_9S_8 and those of (*27*) are in disagreement with Lotgering's (*6*), who reported a Curie–Weiss behavior between 150 and 300°K, with $C_M = 3.96$ and $\theta_p = -50$°K. Heidelberg et al. (*7*) described an increase in $\chi(Co_9S_8)$ from the room-temperature value up to 4.0×10^{-6} emu/g at 1106°K; they interpreted their results, wrongly it would now appear, as showing that Co_9S_8 is probably antiferromagnetic with a Néel point above the decomposition temperature of 1106°K. They also showed that results similar to Lotgering's could be obtained from a sample that had not been properly heat-treated so that it contained sufficient quantities of the decomposition products.

properties of Co_9S_8 and *P* comes from the susceptibility (see above and *27*) and thermoelectric power (*27*) measurements, and from the external-field Mössbauer spectrum of *P* at liquid-helium temperatures (see above and *25*). The small thermoelectric powers, being increasingly negative with increasing temperature, and Pauli paramagnetism down to 4.2°K are typical of metallic conduction by electrons and show that these two sulfides should be considered as broad-band metals, with no resultant magnetic moments on the metal atoms at either site. This is consistent with the fact that no magnetic ordering was observed in natural *P* even at 4.2°K (*1*). These results clearly show that the bonding scheme in Co_9S_8 and *P* must allow for substantial electron delocalization.

Mössbauer Parameters of Synthetic π Phases

The isomer shifts $\delta(f)$ and $\delta(b)$ again are small and in the general range of the corresponding shifts in *P* (Table IV). The $\delta(f)$ values show two trends. First, there is an increase in $\delta(f)$ with increasing a_0 at constant n_d, e.g., in the eu-electronic series *I*, *B*, *K*, *S*. This trend is consistent with the usual volume effect. The overlap between the metal and nonmetal atom wavefunctions decreases with increasing a_0 (cf. the M(f)–S distances in Co_9S_8 above and in *P*, Refs. *22* and *23*), whereby the degree of covalency, and hence the donations of electrons from the nonmetal to the metal atom, are reduced. This results in a decrease of *s*-electron density at the Mössbauer nucleus and an increase in δ, as observed.[6]

The second trend, which is more revealing, may be observed in the series *A*, *B*, *C*, *D*, *E*, *F*. Here $\delta(f)$ *decreases* steadily with increasing a_0, but n_d increases simultaneously from 62 for *A* to 67 for *F*. The decrease in $\delta(f)$ due to increased n_d thus more than compensates the volume effect.

Both trends are seen more clearly in Fig. 9. The gridlines of equal $\delta(f)$ were mapped using the points *R*, *S*, *T*, *U*, *V* to define the scale and the point *A* to define the slope. All points fall on this grid in the positions expected

[6] Similar effects have been observed, for example, in the 3*d* pyrites MS_2 (*28*).

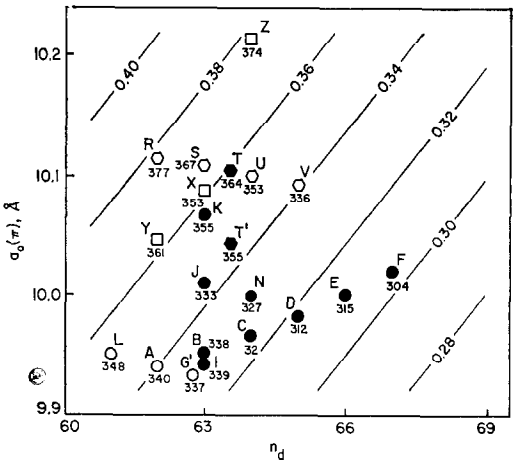

FIG. 9. Variation of the isomer shift $\delta(f)$ at room temperature with $a_0(\pi)$ and the total number n_d of $3d+4d$ electrons per formula unit. Only the decimal digits of the $\delta(f)$ values are shown. For symbols see Fig. 10.

from a_0 and n_d when the uncertainties in the $\delta(f)$ values are taken into account. Moreover the $\delta(f)$ values for the 4*d* phases *X*, *Y*, and *Z* fall more or less where they would be expected if no distinction was made between the 3*d* and 4*d* series. Increasing n_d by unity decreases $\delta(f)$ by about 0.01 mm/sec, while increasing a_0 by 0.1 Å increases $\delta(f)$ by about 0.023 mm/sec. The variation of $\delta(f)$ may then be expressed as $\partial[\delta(f)] \sim -0.01\partial n_d + 0.23\partial a_0$. The negative sign of the first term shows that addition of *d* electrons manifests itself in an increase in *s-electron* density and that *d*-shielding is therefore not the dominant effect in the observed isomer shift.

The second trend shows clearly that the metal-atom neighbors at d_1 have a significant effect on $\delta(f)$, i.e., some of the 3*d* electrons from Co and Ni atoms at 32(f) are delocalized and thus able to affect the isomer shift of an Fe(f) atom.

The $|\Delta|$ values are small, varying from only 0.10 mm/sec for *L* to 0.45 mm/sec for *F* (Table IV). They might at first sight be viewed as values characteristic of complex Fe compounds in which the EFG arises entirely from the lattice contribution q_{latt}. However, in natural *P*, for example, the change in $|\Delta|$ with temperature (Fig. 6) is much larger than would

be expected from a consideration of the change in a_0. Morimoto and Kullerud (*29*) reported an increase in a_0 of ~0.27 Å between 25 and 600°C, i.e., about 4×10^{-4} Å/deg assuming linearity. Using this figure, the expected change in q_{latt} is only about 2½% over a temperature interval of 200°C, whereas the observed changes are 17% between 97°K and room temperature, and a further 37% between room temperature and 200°C. Furthermore, the range of $|\Delta|$ values observed for the π phases is much greater than would be expected if the EFG were entirely due to q_{latt}. The maximum variation in a_0 implies a maximum change in q_{latt} of only about 6%, whereas the increase in $|\Delta|$ from L to F is more than fourfold.

When the $|\Delta|$ values are normalized for volume effect to a constant a_0, that of sample A, by multiplying the observed $|\Delta|$ by $(a_0/a_0^A)^3$, the resulting $|\Delta'|$ values are seen to increase monotonically with n_d (Fig. 10). This plot demonstrates that there must be a substantial contribution to the EFG from the *d*-character of the conduction electrons. Conduction-electron contributions to the EFG have previously been reported by Wertheim et al. (*30*) in the system $Co_{1-x}Fe_xSi$. A discussion of the temperature-dependent

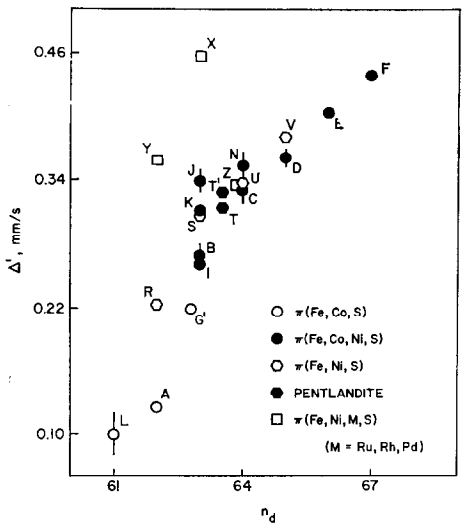

FIG. 10. Variation of the normalized quadrupole splitting $|\Delta'|$ with n_d.

quadrupole splitting can be based on the analysis of Watson et al. (*31*). Their expression for the quadrupole splitting in a metal is $\Delta = e^2qQ$, where $q \sim q_{latt}(1 - \gamma_\infty) + q_{val}(1 - R) - \alpha q_{latt}\, g(E_F)(1 - R)$; γ_∞ and R are the Sternheimer antishielding factors, $g(E_F)$ is the density of states at the Fermi level, and a is a constant dependent upon the symmetry of the conduction-electron orbital. It is not clear *a priori* which of the three terms will dominate in a given case, but values of $\alpha g(E_F)$ from 10 to 100 have been calculated (*31*), indicating this degree of enhancement over lattice terms.

A point-charge lattice sum for P, assuming charges of 2+ on the metal and 2– on the S atoms, shows that q_{latt} is positive at 32(f) and arises entirely from the nearest-neighbor M(f) atoms. This indicates that the conduction-electron term is negative. The external-field Mössbauer spectrum shows e^2qQ in P to be negative, and so the contribution from conduction electrons would appear to be the dominant component of the EFG, as suspected from the temperature dependence of Δ in natural P.

For conduction electrons in a free-electron band, $g(E) = dn/dE \propto (E - E_0)^{1/2}$. Integrating this equation one can relate the number n of electrons in the conduction band to the density of states at the Fermi level: $n \propto g(E_F)^3$. Utilizing the above expression of Watson et al. one obtains $n \propto [A - \Delta(1 + 3da_0/a_0^A)]^3$, which for small values of A (representing lattice and valence contributions to the EFG) reduces to $n \propto -\Delta'^3$.

However, $\delta(f)$ too may be considered to be a measure of n. The following relation may then be expected to hold between $\delta(f)$ and Δ' for small changes in n: $\delta(f)_{calc} \sim (B + C\Delta'^3)(1 + Dda_0/a_0^A)$; the second term allows for the effects of lattice expansion on δ. Fig. 11 shows a plot of the observed versus calculated $\delta(f)$ for the best fit of the parameters ($B = 0.3460$ (15), $C = 0.691(38)$, $D = 6.59(39)$), giving a χ^2 of 16.5 for 13 degrees of freedom. An additional trial allowing for variation in A showed this constant to be very small and ill-determined. Therefore, A was fixed at zero, though, of course, a small positive value is expected here. The smallness of A shows

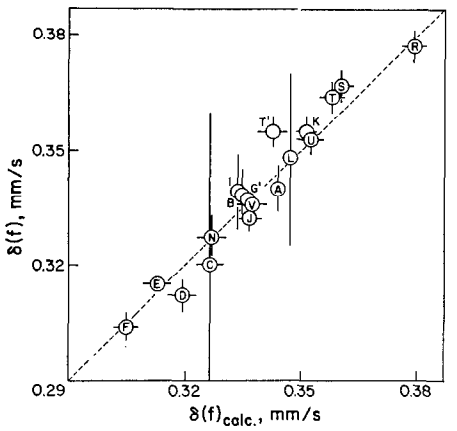

FIG. 11. Correlation of the observed $\delta(f)$ with $\delta(f)_{calc} = (0.346 - 0.691|\Delta'|^3)(1 + 6.59a_0/a_0^4)$.

that the enhancement factor $\alpha g(E_F)$ must be quite large.

The linear relationship of Fig. 11 indeed supports the hypothesis that $n \propto -\Delta'^3$. When the fitted values of $-\Delta'^3 \times 10^4$ are plotted as a function of sample composition (Fig. 12), the lines of constant n are approximately equally spaced and follow, roughly, the lines of constant n_d.

Finally we should like to point out an observation concerning the effect of $4d$ atoms on the Mössbauer parameters. In Fig. 9, the $\delta(f)$ values of X and Y fall on the plot in the positions expected from their a_0 and n_d values while the $|\Delta'|$ values of X and Y are seen to be considerably greater than those of the corresponding isoelectronic $3d$ compositions (Fig. 10). From this, we conclude that the electron density at Fe(f) is independent of the identity (i.e., $3d$ or $4d$) of the 4(b) atom, but the band structure is changed in such a way that the enhancement factor $\alpha g(E_F)$ is increased by 50% or more.

Isomer Shift at 4(b)

Trends in $\delta(b)$ are more difficult to ascertain than those in $\delta(f)$, for the $\delta(b)$ values are less accurate owing to the unfavorable position and intensity of the 4(b) minority singlet relative to the 32(f) quadrupole doublet. The two shifts appear to be related, approximately, by $\delta(b) = \alpha\delta(f) + \beta$ (Fig. 13). The regression coefficients α and β are 1.07(70) and 0.26(24), respectively, for all 17 points, and 1.13(26) and 0.24(9) when A, G', and I are omitted. The correlation coefficients for the two sets are 0.36 and 0.78, respectively, the latter indica-

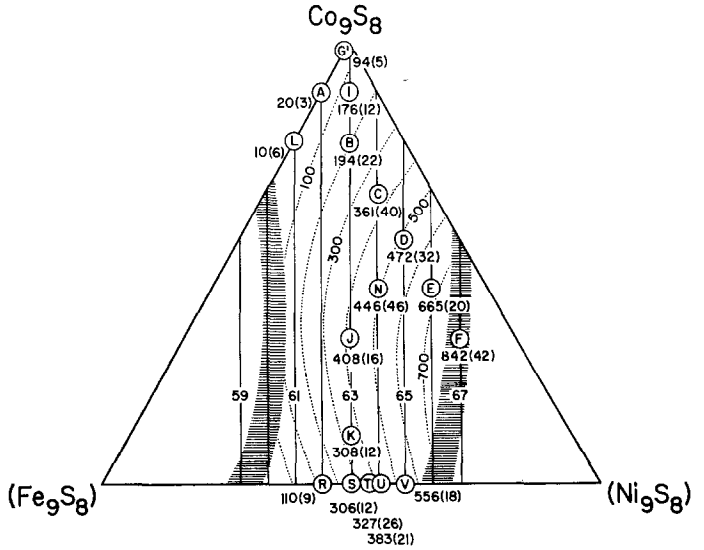

FIG. 12. Contours of constant number n of electrons in the conduction band, as measured by $-\Delta'^3 \times 10^4$, in dependence on sample composition (dotted lines). Full lines, contours of constant n_d. The estimated existence boundaries of the (Fe, Co, Ni)$_9$S$_8$ phase are also shown (shaded zones).

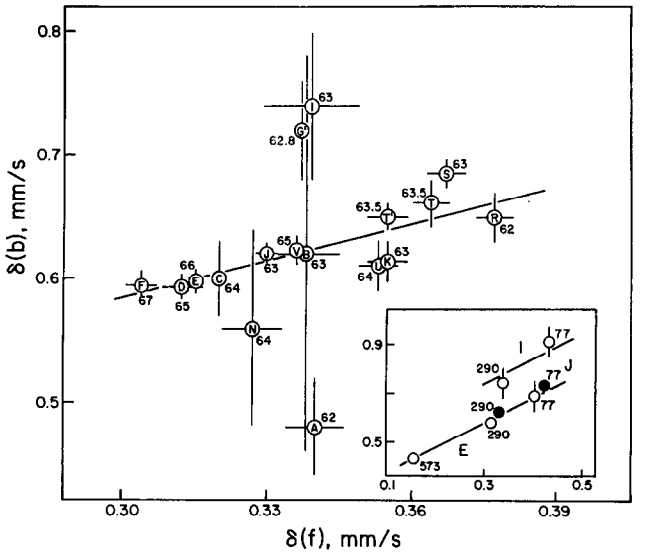

FIG. 13. Correlation of $\delta(b)$ and $\delta(f)$ (room temperature values) in synthetic π phases and pentlandite (n_d values are shown). Inset, dependence of the $\delta(b) - \delta(f)$ correlation on temperature (in °K), samples J (full circles), E and I; the lines drawn through the points have unit slopes.

ting a strong linear correlation. Taking account of the large uncertainties in the $\delta(b)$ values of G' and I, and of the difficulties in extracting $\delta(b)$ from the spectrum of A, it is concluded that the linear dependence of $\delta(b)$ on $\delta(f)$ is real. The proportionality of the two shifts points to a common conduction band, while $\delta(b) > \delta(f)$ follows from $d_{be} > (M^{iv}\text{–}S)$. Within the experimental uncertainty the ratio $\delta(b)/\delta(f)$ does not appear to depend on either a_0 or n_d.

A linear correlation also exists between the $\delta(b)$ and the $\delta(f)$ of a sample measured at different temperatures (E, I, and J, Fig. 13, inset; cf. also Fig. 6). This correlation indicates that the two isomer shifts have the same dependence on the second-order Doppler shift.

Band Model

We will now attempt to devise a model that would account for the facts known to date. While it will be convenient to discuss the band scheme presented in Fig. 14 in terms of Co_9S_8, the scheme applies *mutatis mutandis* to P and the synthetic π phases.

The coordination of the atoms in the Co_9S_8 structure is as follows. The Co(f) atom (site symmetry $3m$), which is tetrahedrally coordinated by one S(c) and three S(e) atoms, has three Co(f) as nearest metal-atom neighbors, at a distance $d_1 \sim 2.5$ Å (Fig. 4). The atoms in the 32(f) complex form isolated Co_8^f cubes, the shortest distance between Co(f) atoms in neighboring cubes being $d_2 \sim 3.5$ Å and thus comparable to the Co–Co distance in metallic Co (see Results). The

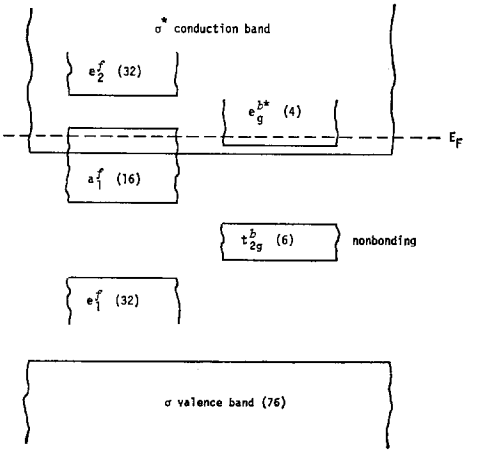

FIG. 14. Provisional schematic band model for the π phases.

nearest Co(*b*) atom is at a much greater distance d_4 of 4.1 Å. Each Co(*b*) atom (site symmetry *m3m*) is octahedrally coordinated by S(*e*) atoms at 2.36 Å; this is very close to the Co–S distance in the metallic ferromagnet CoS_2, 2.32 Å (*3*). The nearest metal-atom neighbors of Co(*b*) are 24 Co(*f*) atoms at d_4. The S(*c*) atom (site symmetry $\bar{4}3m$) is tetrahedrally coordinated by four Co(*f*) atoms, while the coordination figure of S(*e*) is a square pyramid defined by one Co(*b*) and four Co(*f*) atoms.

The band structure of the π phases will undoubtedly turn out to be complicated. The present results, apart from confirming the need for a band-model description, only give limited, if useful, information regarding the conduction band. The very schematic diagram of Fig. 14 is intended to illustrate the general features of the band structure consistent with the observed facts. It is based on a molecular-orbital approach, the molecular orbitals being broadened into bands when the "molecules" are brought together to form the crystal. It is assumed that the 3*s* and 3*p* atomic orbitals of the S(*c*) atom are hybridized to give sp^3 orbitals which are then used to form σ bonds with the Co(*f*) atoms. A similar hybridization of orbitals on the five-coordinated S(*e*) requires formation of sp^3d hybrids using orbitals of symmetry a_1 (two), b_1, and *e*.

The formation of molecular levels between the 4*s* and 4*p* orbitals of Co(*f*) and the hybridized orbitals of S(*e*) and S(*c*) then proceeds in the usual way, resulting in four σ bonding and four σ* antibonding levels per Co(*f*) atom. In the crystal these levels are broadened into the σ valence and σ* antibonding bands separated by an energy gap. The *d* levels of Co(*f*) form two sets of symmetry *e* (labeled $e_1{}^f$ and $e_2{}^f$ in Fig. 14) and one of symmetry a_1. The short d_1 distance between neighboring Co(*f*) atoms in each $Co_8{}^f$ cube suggests that there will be interactions between Co(*f*) neighbors which will broaden the $e_1{}^f$ band and possibly even split it into two subbands, $e_1{}^f(\pi)$ and $e_1{}^{f*}(\pi)$. Electrons in this band will be delocalized around the $Co_8{}^f$ cube and possibly throughout the crystal. In Fig. 14, the bands are not shown closed, as their extent is not known; it may well be that some of the bands are reversed in energy, overlap, or lie below the top of the valence band.

The band structure at the Co(*b*) atom would be expected to be qualitatively similar to the situation which exists in the pyrites (*32*) and sulfospinels (*33*): the 3*d* levels are split into a nonbonding t_{2g}^b and an antibonding e_g^{b*} set.

There are 16 electrons in bonds on S(*c*) and 60 in bonds on S(*e*), totaling 76 electrons in the σ bonds, and six in the nonbonding t_{2g}^b levels. In addition, the $e_1{}^f$ band can accommodate 32 electrons which gives a total of 114 electrons per formula unit. In Co_9S_8 the number of electrons available is 129 while in the hypoelectronic *L* ($n_d = 61$) it is a minimum of 127, so that a further 15 and 13 electrons, respectively, must be accommodated.

In the previous section, we showed that the observed quadrupole splittings are almost entirely due to the conduction-electron term and that the number *n* of electrons in the conduction band is proportional to $-\Delta'^3$. In $L\ \Delta'^3$ approaches zero and so one would expect *n* to be close to zero. For this reason, we propose that the σ* conduction band overlaps the $a_1{}^f$ band as shown in Fig. 14, the composite band containing 13 (in *L*) or more electrons. As n_d is increased the additional electrons go into this *s–d* composite band. Similarly the e_g^{b*} band is immersed in the conduction band. The fact that the free-electron model appears to explain the Δ' results so well can probably be taken as evidence that the σ* band is *broad* and that, as the π-phase composition series is traversed, only a few levels at the bottom of this band are being occupied. The electrons in this band are delocalized through the crystal; this is consistent with the linear relationship between $\delta(b)$ and $\delta(f)$, and possibly also with the observation that in argentian pentlandite[7] the reflectivity is "drastically" reduced relative to that of Fe–Co–Ni pentlandite (cf. *22*, *35*).

A more detailed band scheme will have to await the results of conductivity measurements on suitable π compositions, ordered *and* disordered.

[7] In the argentian pentlandite $Fe_{4.83}Ni_{3.17}Ag_{0.99}S_8$ the Ag atoms were found segregated in the 4(*b*) sites (*23*).

Composition Limits of the π Phase

If the π-phase structure is stabilized by the presence of electrons in the conduction band, then compositions for which this band is completely empty should correspond to the hypoelectronic existence boundary of the π phase. The Mössbauer results would indicate this lower limit to be between $n_d = 60$ and 61.

Approximate existence boundaries of the (Fe, Co, Ni)$_9$S$_8$ phase were originally proposed by Knop and Ibrahim (*9*). For compositions (Fe, Ni)$_9$S$_8$ they were subsequently revised by Shewman and Clark (*21*). Although there are problems with equilibration of the samples at temperatures below 500°C, the combined results of these studies agree sufficiently to place the homogeneity limits of the synthetic (Fe, Ni)$_9$S$_8$ phase at approximately $Fe_{6.0}Ni_{3.0}S_8$ ($n_d = 60$) and $Fe_{3.0(5)}Ni_{6.0(5)}S_8$ ($n_d = 66 \pm 1$). The tentative existence boundaries in the M_9S_8 section of the Fe–Co–Ni–S system at room temperature are shown in Fig. 12. The region they define accommodates all the Fe:Co:Ni ratios reported to date for natural Fe–Co–Ni pentlandites, both from conventional analyses of bulk samples and from microprobe analyses (*8*, *22*, *34*). The hypoelectronic boundary is seen to agree reasonably well with the $n_d = 60$ line compatible with the estimate from the Mössbauer results. The hyperelectronic boundary does not appear to correspond to any uniquely identifiable band occupancy in the present scheme, though the narrowness of the homogeneity range of π(Co, S) seems to suggest the existence of a specific controlling factor.

The extent of the M:S range in the π phases is not known with certainty. For π(Co, S) it is extremely narrow. At room temperature it does not exceed the limits 9.006/8 = 1.1258 and 8.987/8 = 1.1234 (cf. *9*). For synthetic π(Fe, Ni, S) phases the M:S limits reported by Huang (*4*) and by Shewman and Clark (*21*) (samples quenched from 400 and 500°C, respectively) are

Ni:Fe	Ref. (4)	Ref. (*21*)
0.8	1.095(2)–1.142(2)	
1	1.092(2)–1.139(2)	(400°C) 1.111(10)–1.142(10)
		(500°C) 1.092(10)–1.142(10)
1.25	1.096(2)–1.136(2)	

These limits do not appear to depend on the Ni:Fe ratio. Measurement of anion self-diffusion coefficients in π(Co, S) (*17*) has led to the conclusion that the sulfur lattice is practically fully occupied. It is thus reasonable to formulate the nonstoichiometric π phases as $M_{9+\varepsilon}S_8$. Hence, apart from small intrinsic defectiveness, for $\varepsilon > 0$ the 32(*f*) and 4(*b*) sites would be completely filled, with excess M atoms being accommodated interstitially in sites such as 24(*d*), while for $\varepsilon < 0$ the structure would contain metal vacancies.

Rajamani and Prewitt (*22*) have suggested that the tendency of the π(Fe, Ni, S) structure to remain isoelectronic on composition changes produces, in natural Fe–Ni pentlandites, a decrease in the M:S ratio as the Ni content increases, and that this decrease is realized by the formation of vacancies in 32(*f*). This would imply that natural π(Fe, Ni, S) phases with $\varepsilon > 0$ cannot exist for atomic Ni:Fe ratios greater than unity. This conclusion in our view is not entirely borne out by the available analytical data for the mineral, especially when the Co-bearing varieties (*34*) are included, nor is it supported by the observations on the corresponding synthetic phases.

Lattice Parameters and Interatomic Distances

The octahedral distance d_{be} is equal to $a_0(\frac{1}{2} - u)$. A plot of the available u(S) values against a_0 shows that u decreases with increasing a_0, i.e., a_0 and u vary *both* simultaneously so as to either increase or decrease d_{be}. The relationship of d_{be} and a_0 (Fig. 15, top) between 9.9 and 10.6 Å is approximately linear, with $\partial d_{be}/\partial a_0 \sim \frac{1}{2}$, even when a second-degree curve is fitted to the points by least squares. The points for compositions other than Co_8MS_8 and $Fe_4Ni_4MS_8$ require corrections for occupancies of 32(*f*) that are not isoelectronic, but the corrections are quite small. The scatter of the points is due primarily to the considerable uncertainty of the u values that have been obtained from our X-ray and neutron powder intensities, and also to the insufficient accuracy in the determination of the actual occupancy of 4(*b*).

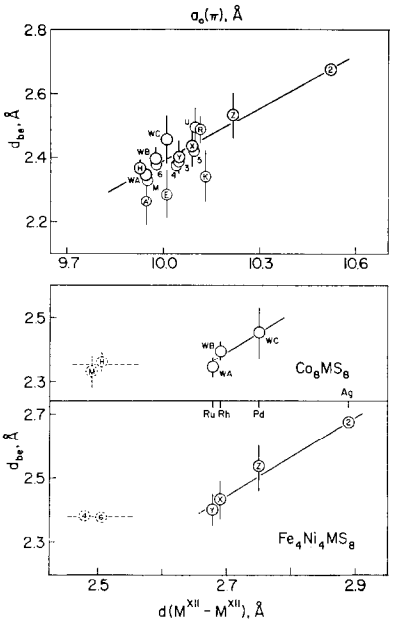

FIG. 15. Variation of the octahedral M–S distance d_{be} with $a_0(\pi)$ (top) and with the shortest metal–metal distance $d^{xii}(M\text{–}M)$ in the pure metals (C.N. 12) (bottom). *2*, argentian *P* (*23*); *3*, natural *P* (*23*); *4*, Frood mine *P* (*22*); *5*, annealed Frood mine *P* (*37*); *6*, Co-rich Outokumpu *P* (*22*). For the 3*d* elements (broken lines) the $d^{xii}(M\text{–}M)$ values are not known with certainty. Top: heavy circles, ordered π phases; thin circles, degree of order uncertain.

The effect of the M(*b*) atom on d_{be}, and hence on a_0 and u, is most clearly seen in the ordered 4*d* series. In both Co_8MS_8 and $Fe_4Ni_4MS_8$ d_{be} increases approximately linearly with $d^{xii}(M\text{–}M)$, the shortest interatomic distance in the pure 4*d* metals at room temperature, and thus with the atomic number of *M* (Fig. 15, bottom); allowing for Ni : Fe ≠ 1 in the Ag pentlandite does not change the correlation significantly. The effective size of M(*b*) thus follows the same sequence as is observed for the pure metals. However, d_{be} is not affected to any extent until the effective size of M(*b*) has reached a certain value, corresponding to a $d^{xii}(M\text{–}M)$ of about 2.7 Å. Below this value d_{be} remains largely independent of M(*b*), as is seen from the d_{be} values of *H*, *M*, *K*, *E* and the natural pentlandites, even though the $d^{xii}(M\text{–}M)$ distances in the 3*d* metals are in the vicinity of 2.5 Å, i.e., *below* Ru and Rh by about the same amount as Pd is *above* Ru and Rh (Fig. 15, bottom),[8] so that a further decrease in d_{be} might be expected. However, the *small-scale* variation in d_{be} from one 3*d* element to another may well turn out to follow the same trend as the variation observed for the 4*d* atoms, i.e., an increase in d_{be} with the atomic number of M(*b*) as a result of the progressive filling of the conduction band. Some evidence for this is provided by Rajamani's (*37*) observation that d_{be} in natural *P* increased on annealing from 2.377 to 2.418 Å, corresponding to an increased Ni occupancy of 4(*b*) (cf. *1*), while the *average* M^{iv}–S distance remained the same, 2.232 Å at room temperature.

To explain the observed variation of a_0 with composition in π(Fe, Co, Ni, S) phases (*8*, *9*, *21*; Table I) it is necessary to assume that the effective sizes of the 3*d* atoms in the majority 32(*f*) sites follow the sequence Fe > Ni > Co. A similar size sequence has been observed, for example, in the metallic but nonmagnetic ThM_2Si_2 phases (M = Fe, Co, Ni) (cf. *36*, p. 161). The only M^{iv}–S distances in the π phases known with some certainty are those in Co_9S_8, $d_{fc} = 2.122(15)$ Å and $d_{fe} = 2.231(22)$ Å (cf. Results). Only the average values of d_{fc} and d_{fe} are known for Fe and Ni, as bulk π-Fe_9S_8 and π-Ni_9S_8 have not been reported and possibly do not exist. Two independent determinations of d_{fc} and d_{fe} in natural *P* have resulted in a very close agreement: 2.154(1) and 2.258(1) Å, respectively, in (*22*), and 2.156(2) and 2.257(2) Å, respectively, in (*23*); the small difference in the compositions of the two samples seems unimportant. Thus, the average (Fe, Ni)^{iv}–S and Co^{iv}–S distances differ by only about 0.03 Å at Ni : Fe = 1 and possibly by less. The smallness of the variation of d_{fc} and d_{fe} with composition, the anisotropy of the 32(*f*) site, and the nonlinear increase of a_0 with the Fe : Ni

[8] The effective sizes of the Fe, Co, and Ni atoms in metallic materials depend upon the particular situation; even their sequence may vary from alloy to alloy or from compound to compound (*36*, p. 158). Metallic Fe, Co, and Ni are unsuitable for determining the effective atomic sizes for use in the present investigation. At room temperature they are far below their respective Curie temperatures, and α-Fe is b.c.c. while Co and Ni are f.c.c.

ratio (and thus with decreasing n_d) in synthetic π(Fe, Ni, S) (*8*, *9*, *21*) would all make any attempt at explanation speculative at present.

Acknowledgments

We wish to express our gratitude to the following individuals and agencies: the staff of the Neutron Physics Branch, Atomic Energy of Canada Limited, for making available the neutron diffraction facilities and for assistance with the experiments; Dr. R. E. Meads and Dr. W. G. Parker (University of Exeter) for obtaining the Mössbauer spectrum of pentlandite in an external magnetic field; Dr. M. H. Jericho for the use of his magnetic-susceptibility apparatus; Dr. T. C. Gibb (University of Leeds) for supplying a copy of his program for simulation of external-field Mössbauer spectra; and The International Nickel Company of Canada Limited, for providing us with generous quantities of mineral material and for awarding an INCO Graduate Research Fellowship to one of us.

This work was supported by grants in aid of research from the National Research Council of Canada and the Geological Survey of Canada.

References

1. O. KNOP, C.-H. HUANG, AND F. W. D. WOODHAMS, *Amer. Miner.* **55**, 1115 (1970).
2. SUTARNO, Ph.D. thesis, Nova Scotia Technical College, Halifax, Nova Scotia (1965).
3. K. I. G. REID, Ph.D. thesis, Dalhousie University, Halifax, Nova Scotia (1968).
4. C.-H. HUANG, Ph.D. thesis, Dalhousie University, Halifax, Nova Scotia (1970).
5. V. G. KUZNETSOV, A. A. ELISEEV, Z. S. SHPAK, K. K. PALKINA, M. A. SOKOLOVA, AND A. V. DMITRIEV, *Vopr. Met. i Fiz. Poluprovod., Akad. Nauk SSSR, Trudy 4-go Soveshch., Moscow*, 159 (1961); *Chem. Abstr.* **56**, 5444 (1962).
6. F. K. LOTGERING, *Philips Res. Repts.* **11**, 337 (1956).
7. R. F. HEIDELBERG, A. H. LUXEM, S. TALHOUK, AND J. J. BANEWICZ, *Inorg. Chem.* **5**, 194 (1966).
8. O. KNOP, M. A. IBRAHIM, AND SUTARNO, *Canad. Miner.* **8**, 291 (1965).
9. O. KNOP AND M. A. IBRAHIM, *Canad. J. Chem.* **39**, 297 (1961).
10. O. KNOP, K. I. G. REID, SUTARNO, AND Y. NAKAGAWA, *Canad. J. Chem.* **46**, 3463 (1968).
11. O. KNOP, F. BRISSE, L. CASTELLIZ, AND SUTARNO, *Canad. J. Chem.* **43**, 2812 (1965).
12. D. T. CROMER AND J. T. WABER, *Acta Crystallogr.* **18**, 104 (1965).
13. "International Tables for X-ray Crystallography," Vol. 3, Kynoch Press, Birmingham (1962).
14. D. T. CROMER, *Acta Crystallogr.* **18**, 17 (1965).
15. SUTARNO, O. KNOP, AND K. I. G. REID, *Canad. J. Chem.* **45**, 1391 (1967).
16. S. GELLER, *Acta Crystallogr.* **15**, 1195 (1962).
17. J. R. STUBBLES, Ph.D. thesis, Imperial College, University of London (1957).
18. V. G. KUZNETSOV, M. A. SOKOLOVA, K. K. PALKINA, AND Z. V. PAPOVA, *Izv. Akad. Nauk SSSR, Neorg. Mater.* **1**, 675 (1965); *Inorg. Mater.* **1**, 617 (1965).
19. G. PANNETIER, G. BUGLI, AND P. COURTINE, *Bull. Soc. Chim. France* 107 (1962).
20. O. KNOP, *Chem. and Ind.* 739 (1962).
21. R. W. SHEWMAN AND L. A. CLARK, *Canad. J. Earth Sci.* 7, 67 (1970).
22. V. RAJAMANI AND C. T. PREWITT, *Canad. Miner.* **12**, 178 (1973).
23. S. R. HALL AND J. M. STEWART, *Canad. Miner.* **12**, 169 (1973).
24. C.-H. HUANG AND O. KNOP, *Canad. J. Chem.* **49**, 598 (1971).
25. D. J. VAUGHAN AND M. S. RIDOUT, *J. Inorg. Nucl. Chem.* **33**, 741 (1971).
26. T. C. GIBB, private communication.
27. M. G. TOWNSEND, J. L. HORWOOD, R. J. TREMBLAY, AND L. G. RIPLEY, *Phys. Status Solidi (a)* **9**, K137 (1972).
28. P. K. GALLAGHER, J. B. MACCHESNEY, AND R. C. SHERWOOD, *J. Chem. Phys.* **50**, 4417 (1969).
29. N. MORIMOTO AND G. KULLERUD, *Carnegie Inst. Wash. Year Book* **63**, 204 (1964).
30. G. K. WERTHEIM, J. H. WERNICK, AND D. N. E. BUCHANAN, *J. Appl. Phys.* **9**, 3333 (1966).
31. R. E. WATSON, A. C. GOSSARD, AND Y. YAFET, *Phys. Rev.* **140**, A375 (1965).
32. T. A. BITHER, R. J. BOUCHARD, W. H. CLOUD, P. C. DONOHUE, AND W. J. SIEMONS, *Inorg. Chem.* **7**, 2208 (1968).
33. J. B. GOODENOUGH, *J. Phys. Chem. Solids* **30**, 261 (1969).
34. D. C. HARRIS AND E. H. NICKEL, *Canad. Miner.* **11**, 861 (1972).
35. S. D. SCOTT AND E. GASPARRINI, *Canad. Miner.* **12**, 165 (1973).
36. W. B. PEARSON, "Crystal Chemistry and Physics of Metals and Alloys," Wiley, New York (1972).
37. V. RAJAMANI, personal communication.
38. F. W. D. WOODHAMS, P. S. WHITE, AND O. KNOP, *J. Solid State Chem.* **5**, 334 (1972).